Electronic Supplementary Material (ESI) for Chemical Communications

Electronic Supplementary Information

The luminescence properties of linear vs. kinked aurophilic 1-D chains of bis(dithiocarbamato)-gold(I) complexes

Ryan J. Roberts,[†] Nicolas Bélanger-Desmarais,[‡] Christian Reber,*[,‡] and Daniel B. Leznoff*[,†]

Contents

List of Figures

Figure S 9. Pressure-Dependent Raman spectra (lexc = 785 nm)4 of [Au2(edtc)2]n for the 880 to 1200 cm-1 region (edtc denotes N,N-diethyldithiocarbamate). Pressures are (bottom to top): 1 bar, 4, 7, 9, 11, 13, 16, 19, 21, 24, 28 kbar. Peak assignments are based on published IR analyses9-11.

Figure S 10. Pressure-Dependent Raman spectra (lexc = 785 nm)4 of [Au2(edtc)2]n (left panel) and of [Au2(dopdtc)2]n (right panel) for the 880 to 1200 cm-1 region. Peak assignments are based on published IR analyses9-11.

Figure S 11. Pressure-Dependent Raman spectra (lexc = 785 nm) of [Au2(dopdtc)2]n (Top panel) and of [Au2(edtc)2]n (Bottom panel)4 for the 500 to 700 cm-1 region. Pressures for the bottom panel are (bottom to top): 1 bar, 4, 7, 9, 11, 13, 16, 19, 21, 24, 28 kbar. The bottom panel illustrates well the possible consequences of applying pressure on the linear polymeric chains of [Au2(edtc)2]n (broadening of the peaks as a result of structure degradation and appearance of a new peak at ca. 610 cm-1).

Figure S 12. Isodensity plots (0.02 atomic units) of HOMO (Left-hand side) and LUMO (Right-hand side) molecular orbitals for a linear gold (I) dithiocarbamate compound ([Au2(edtc)2]2, upper panel) and for a "zig-zag" gold (I) dithiocarbamate compound ([Au2(dopdtc)2]2, bottom panel). These were obtained from DFT calculations on a tetramer (PBEPBE14-16/Lanl2dz17, Gaussian 03 (Gaussian Inc.)12) with the 5.08 release of the GaussView software (Gaussian Inc.)12. Hydrogens were omitted to clarify the picture. The color code used for the atoms is the following: Carbon: grey, Nitrogen: blue, Sulphur: orange and Gold: yellow.

Figure S 13. Explanation of the observed Red-shift4 with increasing pressure (Top: [Au2(dopdtc)2]2 and Bottom: [Au2(edtc)2]2). The following scheme highlights the fact that [Au2(dopdtc)2]2 experiences a smaller red-shift with increasing pressure because of the nature of the LUMO orbital, which makes this orbital insensitive to a decrease of the interdimer Au-Au bond length.

Figure S 14. Isodensity plots (0.02 atomic units) of the LUMO+16 molecular orbital of [Au2(dopdtc)2]2 obtained from DFT calculations on a tetramer segment of the polymer(PBEPBE14-16/Lanl2dz17, Gaussian 03 (Gaussian Inc.)12) with the 5.08 release of the GaussView software (Gaussian Inc.)12. Hydrogens were omitted to clarify the picture. The color code used for the atoms is the following: Carbon: grey, Nitrogen: blue, Sulphur: orange and Gold: yellow. This molecular orbital exhibits a Au-Au σ–βονδινγ interaction between the dimers. The character of this interaction is really similar to what is found for the LUMO molecular orbital of another Gold(I) dithiocarbamate polymer4, [Au2(edtc)2]2.

Figure S 15. Molecular Orbitals Energy diagram obtained from DFT calculations on tetramers of two Gold(I)dithiocarbamate polymer (PBEPBE14-16/Lanl2dz17, Gaussian 03 (Gaussian Inc.)12). The dashed line illustrates the fact that the orbital with a similar character for the interaction between the dimers (s-bonding) is higher in energy with respect to the HOMO for the studied system (red) than for a linear Gold(I)dithiocarbamate polymer (blue) found in literature4.

Figure S 16. Solution absorption and luminescence spectra of $[Au_2(edtc)_2]$ and $[Au_2(dopdtc)_2]$.

List of Tables

Experimental

General Procedures. All reactions were carried out in air unless otherwise stated. Benzyl potassium, KCH_2Ph,[1] and chloro(tetrahydrothiophene)gold(I), AuCl(tht),[2] were synthesized according to literature procedures. Tetrahydrofuran (THF) was distilled over a dinitrogen atmosphere from sodium/benzophenone. All other reagents were obtained from commercial sources and used as received.

Infrared spectra were recorded on a Thermo Nicolet Nexus 670 FTIR spectrometer equipped with a Pike MIRacle attenuated total reflection (ATR) sampling accessory.

NMR spectra were recorded at 294 K, unless otherwise stated, on either a 500 MHz Bruker Avance III spectrometer, or a 600 MHz Bruker Avance II spectrometer with a 5 mm QNP cryoprobe. All ^{1}H and ^{13}C NMR shifts are reported in ppm relative to the impurity of internal solvent: specifically, CD_2Cl_2 at $\delta = 5.32$ ppm or d^7-DMF at $\delta = 2.77$ ppm for ^{1}H and $CDCl_3$ at $\delta = 54.0$ ppm or d^7-DMF at $\delta = 29.50$ ppm for ^{13}C.

Microanalyses (C, H, N) were performed by Frank Haftbaradaran at Simon Fraser University on a Carlo Erba EA 1110 CHN elemental analyzer.

The solid-state reflectance spectrum of the title compound was measured on a Cary 6000i UV-Vis-NIR spectrophotometer with a praying mantis accessory. Raman and luminescence spectra were measured with a Renishaw 3000 Raman imaging microscope equipped with a Peltier-cooled CCD camera. Excitation sources were a 488 nm argon ion laser for the Temperature-dependent luminescence experiments, a 514 nm

argon ion laser for the Pressure-dependent luminescence experiments and a 785 nm diode laser for the Raman experiments. The microscope was used to focus light onto a spot of approximately 1 μm in diameter and to collect the scattered light. Low-temperature Raman and luminescence experiments were performed by coupling a Linkam coldfinger cryostat to the apparatus with liquid nitrogen used as coolant. Pressure-dependent measurements on solid samples in nujol were made with a diamond-anvil cell (DAC, High-Pressure Diamond Optics). The ruby R_1 line method[3] was used to calibrate the hydrostatic pressure inside the gasketed cell. All pressure-induced phenomena reported here are reversible upon gradual release of external pressure.

Synthesis

K(dopdtc): Synthesis was carried out by the modification of a literature procedure[4] using standard inert atmosphere Schlenk techniques. A 500 mL side arm round bottom flask was charged with KCH_2Ph (1.94 g, 14.9 mmol) and dissolved in 160 mL of THF. The solution was then allowed to cool with the aid of an ice bath for approximately 30 minutes. 2,2′-Dipyridylamine (2.50 g, 14.6 mmol) was degassed *in vacuo* for approximately 30 minutes after which it was dissolved in 50 mL of THF and added to the KCH_2Ph solution via syringe, upon which the originally dark red KCH_2Ph solution turned to a pale yellow end point. The reaction was allowed to stir for 18 h at room temperature after which the flask was cooled to -78°C to precipitate potassium 2,2′-dipyridylamide. Carbon disulfide, CS_2 (3 mL, 50 mmol) was then added to the slurry and the mixture stirred at -78°C for 6 h, affording **K(dopdtc)**, $(C_5H_4N)_2NCS_2K$, as a yellow slurry. The bath was removed and 150 mL of diethyl ether (Et_2O) was added to the slurry, which was brought to approximately -10°C to precipitate out any solubilized product. The yellow powder was then filtered and washed with an additional 150 mL of Et_2O. Yield: 4.10 g, 98.3%. K(dopdtc) should be stored in a moisture-free environment; exposure to humidity resulted in decomposition involving formation of the starting material 2,2′-dipyridylamine. **K(dopdtc)** shows moderate decomposition in protic solvents such as MeOH and H_2O over several minutes. Anal. Calcd. For $C_{11}H_8KN_3S_2 \cdot ½H_2O$: C, 44.87%; H, 3.08%; N, 14.27%. Found: C, 44.84%; H, 3.01%; N, 12.86%. Due to the highly hygroscopic nature of the compound, obtaining

accurate elemental analysis was challenging. IR (ATR, cm^{-1}): 1590 (m), 1567 (w), 1470 (w), 1464 (m), 1431 (s), 1300 (m), 1283 (m), 1254 (m), 1235 (m), 1178 (w), 1149 (w), 1098 (w), 1056 (s), 995 (m), 910 (m), 834 (w), 774 (w), 747 (w), 737 (w)

PPN(dopdtc): Bis(triphenylphosphine)iminium chloride (PPNCl) (604 mg, 1.05 mmol) was dissolved in 120 mL of H_2O, to which K(dopdtc) (300 mg, 1.05 mmol) in 20 mL H_2O was added, generating an immediate yellow precipitate. The slurry was immediately filtered, yielding a yellow powder of $[(C_6H_5)_3P)_2N][(C_5H_4N)_2NCS_2]$, PPN(dopdtc). Yield: 800 mg, 97%. Crystals of **PPN(dopdtc)** suitable for single crystal X-ray diffraction were grown via recrystallization from a saturated solution of refluxing MeOH which was slowly cooled to room temperature. Anal. Calcd. for $C_{47}H_{38}N_4P_2S_2$: C 71.92 %, H 4.88 %, N 7.14 %; Found C 71.91 %, H 4.99 %, N 7.24 %. ^{1}H NMR (600 MHz, CD_2Cl_2, 25°C) δ ppm: 7.30 (2H, ddd), 7.47-7.49 (24H, m), 7.57 (2H, m), 6.67 (6H, m), 7.82 (2H, ddd), 8.50 (2H, ddd) $^{13}C\{^1H\}$ NMR (600 MHz, $CDCl_3$, 25°C) δ ppm: 119.81, 122.92, 127.03 (d, J = 108 Hz), 129.75 (m), 132.15 (m), 134.07, 135.89, 147.92, 160.89, 221.95 (NCS_2) IR (ATR, cm^{-1}): 3053 (w), 3006 (w), 1587 (m), 1567 (w), 1470 (w), 1438 (m), 1434 (m), 1427 (s), 1309 (s), 1295 (s), 1275 (m), 1232 (m), 1182 (w), 1153 (m), 1145 (m), 1113 (s), 1087 (w), 1074 (w), 1057 (s), 1044 (m), 996 (m), 909 (w), 872 (w), 833 (w), 797 (w), 777 (w), 757 (w), 751 (w), 743 (w), 723 (s). **PPN(dopdtc)** is not significantly hygroscopic.

[Au(dopdtc)]$_2$: **PPN(dopdtc)** (3.35 g, 4.26 mmol) and AuCl(tht) (1.64 g, 5.12 mmol) were dissolved in 40 mL of CH_2Cl_2 to form a yellow solution which was stirred at room temperature for 18 h. The solvents were removed *in vacuo*, leaving a very fine dark red powder. The powder was then centrifuged in CH_2Cl_2 and the resultant supernatant was discarded. The remaining red powder was suspended in Et_2O, filtered, and dried to give a bright orange powder of **[Au(dopdtc)]$_2$**. Yield: 1.28 g, 53.4% with respect to AuCl(tht). Crystals of **[Au(dopdtc)]$_2$** suitable for single crystal X-ray diffraction were grown via vapour diffusion of MeOH into a saturated DMF solution. Anal. Calcd. for $C_{22}H_{16}Au_2N_6S_4$: C 29.80 %, H 1.82 %, N 9.48 %; Found C 29.89 %, H 1.61 %, N 9.35 %. ^{1}H NMR (600 MHz, d^7-DMF, 25°C) δ ppm: 7.50 (4H, dd), 7.86 (4H, d), 8.07 (4H, dt), 8.58 (4H, dd) $^{13}C\{^1H\}$ NMR (600 MHz, d^7-DMF, 25°C) δ ppm: 123.99, 124.97, 139.80, 150.08,

156.62, 212.73 (NCS_2) IR (ATR, cm^{-1}): 3078 (w), 3047 (w), 1584 (s), 1461 (s), 1427 (s), 1330 (s, br), 1284 (s), 1196 (w), 1149 (w), 1096 (w), 1057 (m), 1041 (m), 995 (m), 902 (w), 779 (w), 770 (w), 746 (m), 743 (m), 733 (w)

X-ray Crystallography

Crystals of PPN(dopdtc) and $[Au(dopdtc)]_2$ were coated in Paratone oil and mounted onto a MiTeGen Micromount and the data was collected at room temperature. Selected bond lengths and angles are shown in Table S1 and additional crystallographic information can be found in Table S2.

All diffraction data were processed with the Bruker Apex II software suite. The structures were solved with SIR92.[5] Subsequent refinements were performed using CRYSTALS.[6] The coordinates and anisotropic displacement parameters for the non-hydrogen atoms were refined. Hydrogen atoms were placed in geometrically calculated positions and refined using a riding model, and a constrained isotropic thermal parameter. The final refinement was conducted using observed data ($I_o \geq 2.5\sigma(I_o)$). Diagrams were prepared using ORTEP-3[7] and POV-RAY.[8]

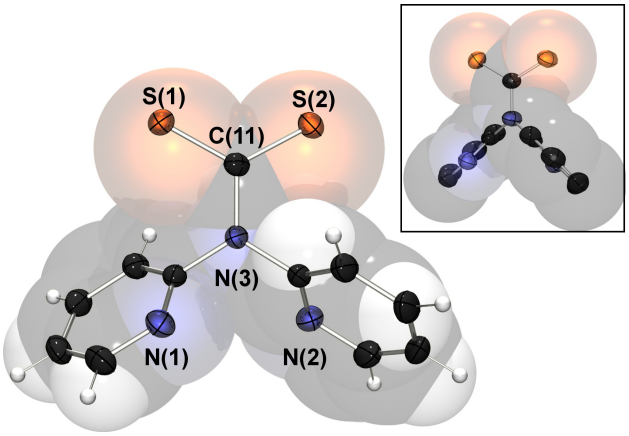

Figure S 1. Crystal structure of the $dopdtc^-$ anion in PPN(dopdtc) viewed perpendicular to the NCS_2 plane (space filling view underlaid to accentuate the ring orientations) and (insert) viewed illustrating the relative orientation of the pyridyl rings. Hydrogen atoms removed for clarity.

Table S 1. Selected bond lengths and angles.

Bond lengths (Å)		Bond angles (°)	
PPN(dopdtc)			
N(3) – C(11)	1.401(2)	S(1) – C(11) – S(2)	124.32(10)
C(11) – S(1)	1.6878(18)	N(3) – C(11) – S(1)	117.54(12)
C(11) – S(2)	1.6891(17)	N(3) – C(11) – S(2)	118.13(13)
[Au(dopdtc)]$_2$			
Au(1) – Au(2)	2.9925(3)	Au(1)' – Au(1) – Au(2)	165.552(12)
		Au(1) – Au(2) – Au(2)'	107.894(10)
Au1			
N(2) – C(11)	1.328(6)	S(1) – C(11) – S(2)	128.1(3)
C(11) – S(1)	1.706(5)	N(2) – C(11) – S(1)	116.0(3)
C(11) – S(2)	1.721(5)	N(2) – C(11) – S(2)	115.9(4)
Au(1) – Au(1)'	2.7932(4)	S(1)^t – Au(1) – S(2)	172.71(5)
Au(1) – S(1)	2.2829(14)		
Au(1) – S(2)	2.2849(14)		
Au2			
N(5) – C(22)	1.343(6)	S(3) – C(22) – S(4)	127.8(3)
C(22) – S(3)	1.706(5)	N(5) – C(22) – S(3)	115.7(4)
C(22) – S(4)	1.722(5)	N(5) – C(22) – S(4)	116.2(4)
Au(2) – Au(2)'	2.8161(4)	S(3) – Au(2) – S(4)'	172.98(5)
Au(2) – S(3)	2.2824(14)		
Au(2) – S(4)'	2.2864(13)		

(') Symmetry operation: $-x, -y, -z$.

Table S 2. Crystallographic data for PPN(dopdtc) and $[Au(dopdtc)]_2$

	PPN(dopdtc)	**$[Au(dopdtc)]_2$**
Empirical formula	$C_{47}H_{38}N_4P_2S_2$	$C_{22}H_{16}Au_2N_6S_4$
Formula weight ($g \cdot mol^{-1}$)	784.92	886.61
Crystal System	Monoclinic	Triclinic
Space Group	$P2_1/c$	$P\bar{1}$
a (Å)	15.6667(2)	9.89190(10)
b (Å)	15.4415(2)	10.6931(2)
c (Å)	17.7248(2)	12.77110(10)
α (°)	90	81.1430(10)
β (°)	107.7150(10)	77.83
γ (°)	90	74.36
V (Å^3)	4084.61(9)	1264.85(3)
Z	4	2
T (K)	293	293
ρ_{calcd} ($g \cdot cm^{-3}$)	1.276	2.328
μ (mm^{-1})	0.247	11.939
Reflections $[I_0 \geq 2.50\sigma(I_0)]$	6842	4837
R, R_w $[I_0 \geq 2.50\sigma(I_0)]$	0.0367, 0.0380	0.0255, 0.0220
Goodness of fit	1.1107	1.1245

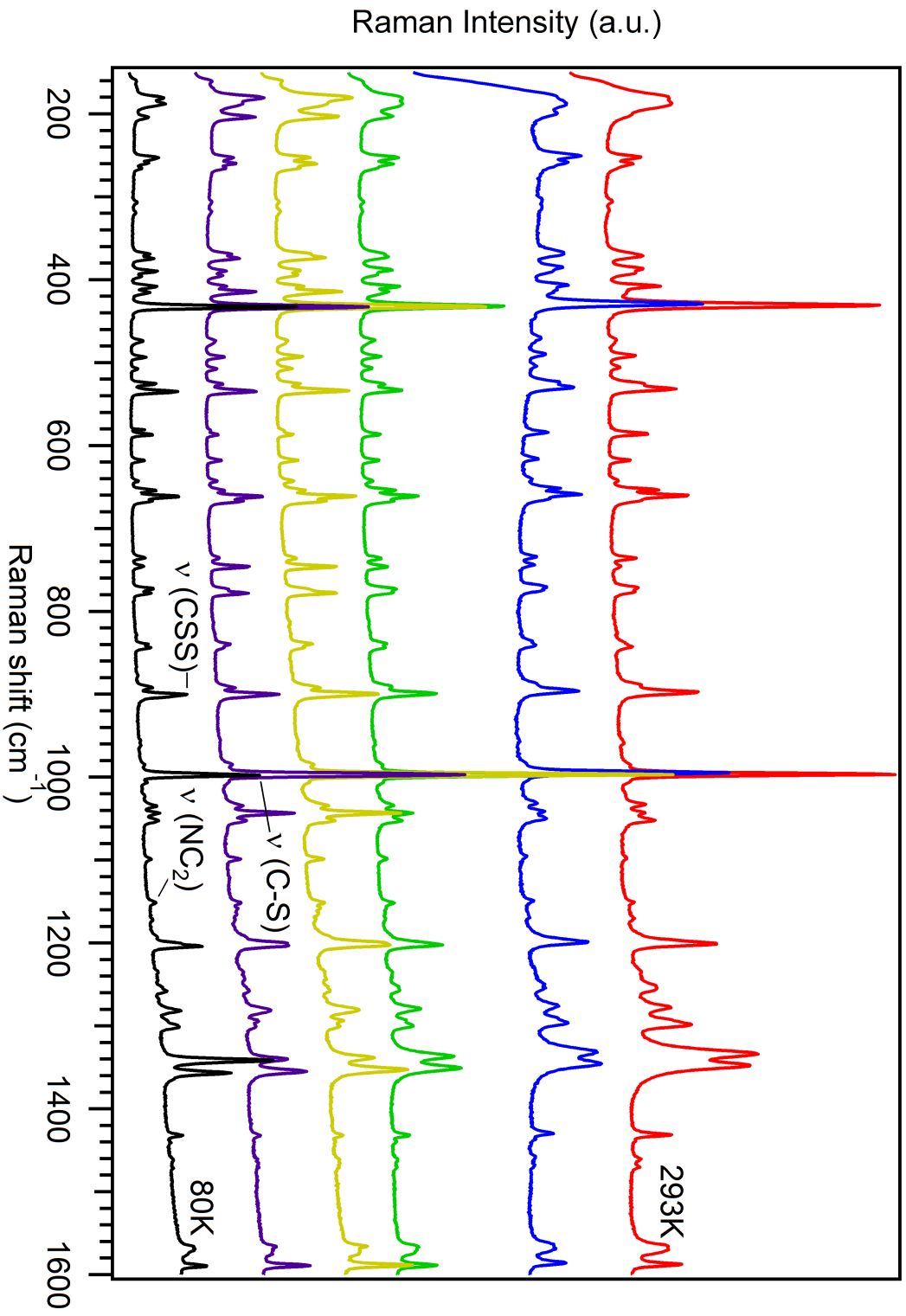

Figure S 2. Raman spectra at variable temperature (λ_{exc} = 785 nm) for $[Au_2(dopdtc)_2]_n$ measured in chronological order of increasing temperature. Spectra are offset along the y-axis for clarity. Temperatures are (top to bottom): 293, 280, 230, 180, 130, 80 K. Peaks are assigned based on comparisons with published IR spectra[9-11] of dtc compounds and their respective metal complexes.

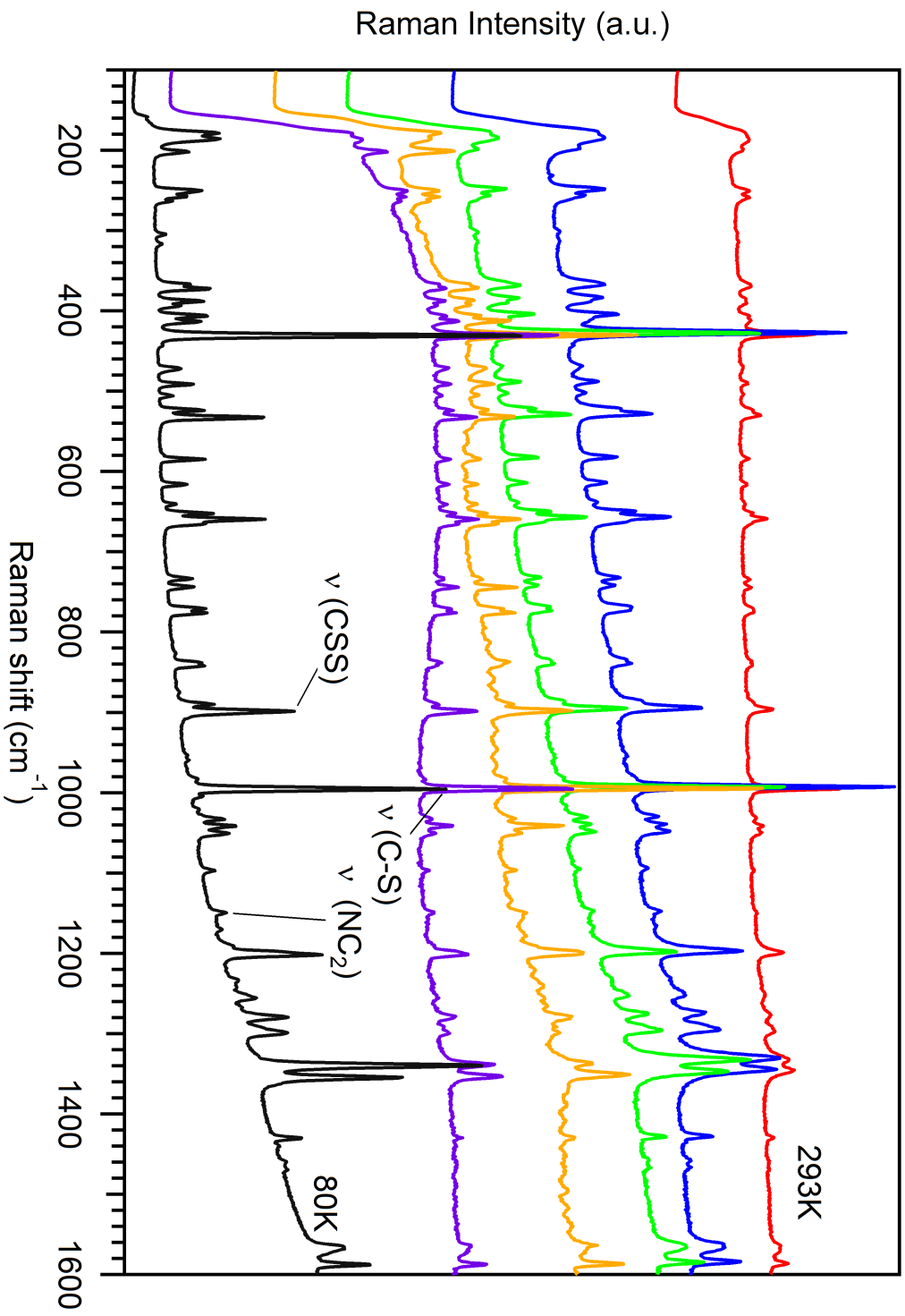

[Figure S 3. Raman spectra at variable temperature (λ_{exc} = 785 nm) for $[Au_2(dopdtc)_2]_n$ in chronological order of decreasing temperature. Spectra are offset along the y-axis for clarity. Temperatures are (top to bottom): 293, 280, 230, 180, 130, 80 K. Peaks were assigned based on comparisons with published IR spectra[9-11] of dtc compounds and their respective metal complexes.

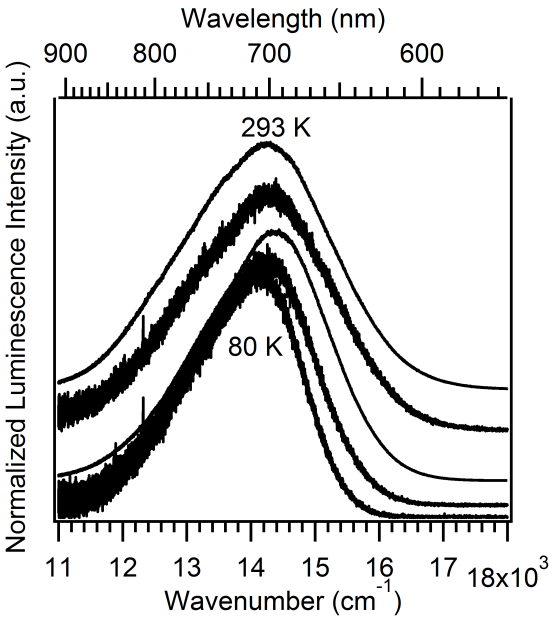

Figure S 4. Normalized luminescence spectra of $[Au_2(dopdtc)_2]_n$ at variable temperature (λ_{exc} = 488 nm). Temperatures are (top to bottom): 293, 280, 180, 130, 80 K. Spectra are offset along the y-axis for clarity and corrected for system response.

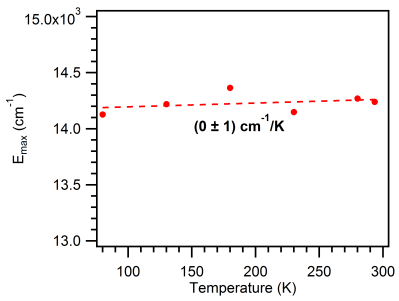

Figure S 5. Luminescence maxima at variable temperature for $[Au_2(dopdtc)_2]_n$.

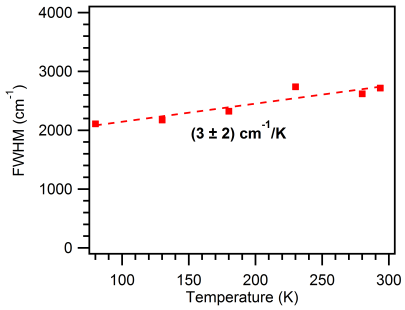

Figure S 6. Full width at half maximum (FWHM) of the luminescence band measured at variable temperature for $[Au_2(dopdtc)_2]_n$.

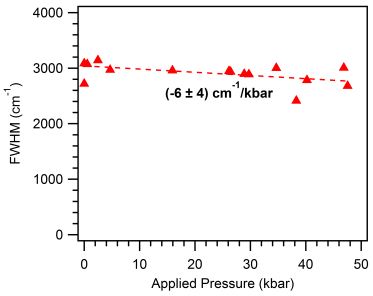

Figure S 7. Full width at half maximum (FWHM) of the luminescence band measured at variable pressure for $[Au_2(dopdtc)_2]_n$.

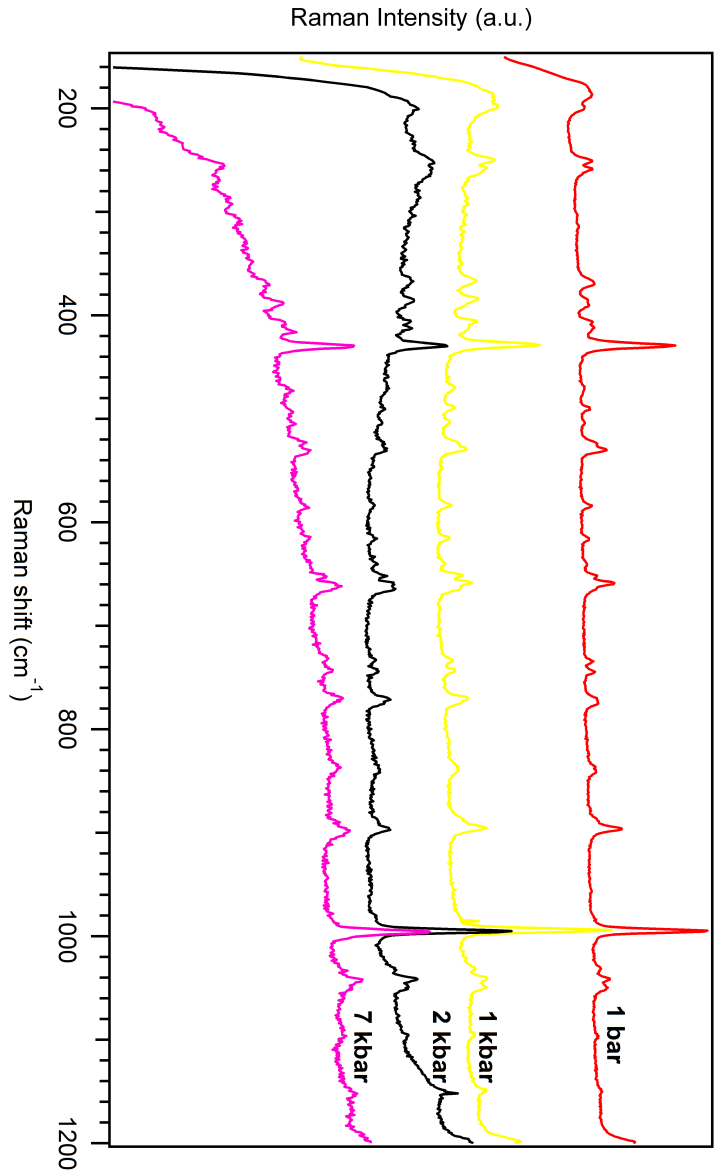

Figure S 8. Pressure-dependent Raman spectra (λ_{exc} = 785 nm) for $[Au_2(dopdtc)_2]_n$. The pressures are given above the corresponding spectra. Spectra are offset along the y-axis for clarity.

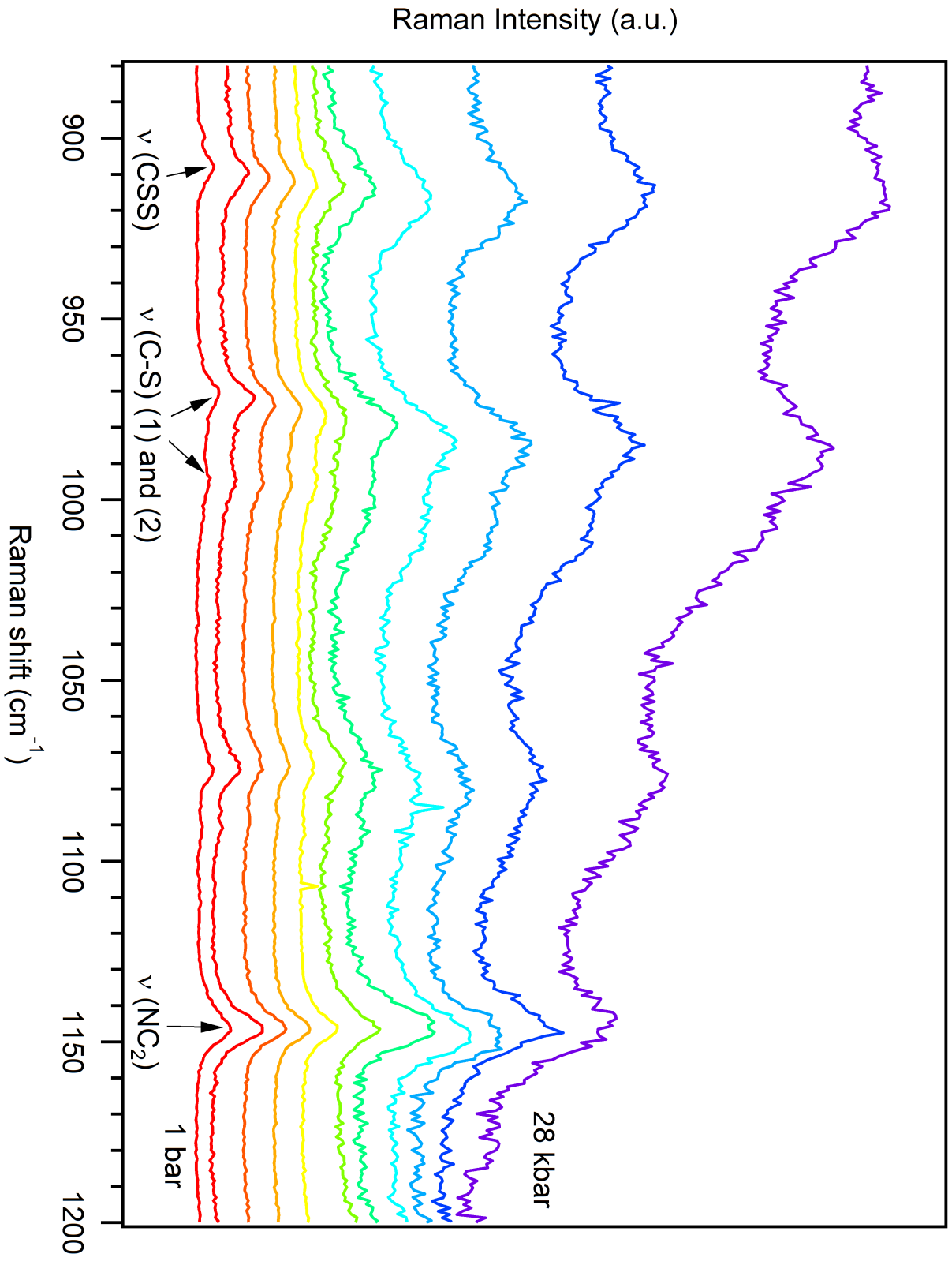

Figure S 9. Pressure-Dependent Raman spectra (λ_{exc} = 785 nm)[4] of $[Au_2(edtc)_2]_n$ for the 880 to 1200 cm^{-1} region (edtc denotes N,N-diethyldithiocarbamate). Pressures are (bottom to top): 1 bar, 4, 7, 9, 11, 13, 16, 19, 21, 24, 28 kbar. Peak assignments are based on published IR analyses[9-11].

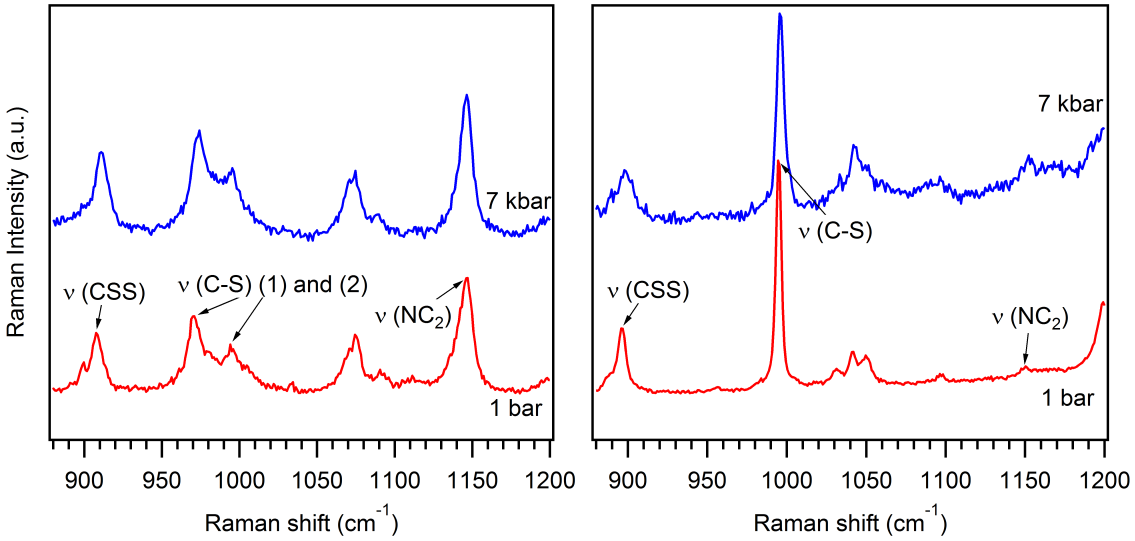

Figure S 10. Pressure-Dependent Raman spectra (λ_{exc} = 785 nm)[4] of $[Au_2(edtc)_2]_n$ (left panel) and of $[Au_2(dopdtc)_2]_n$ (right panel) for the 880 to 1200 cm^{-1} region. Peak assignments are based on published IR analyses[9-11].

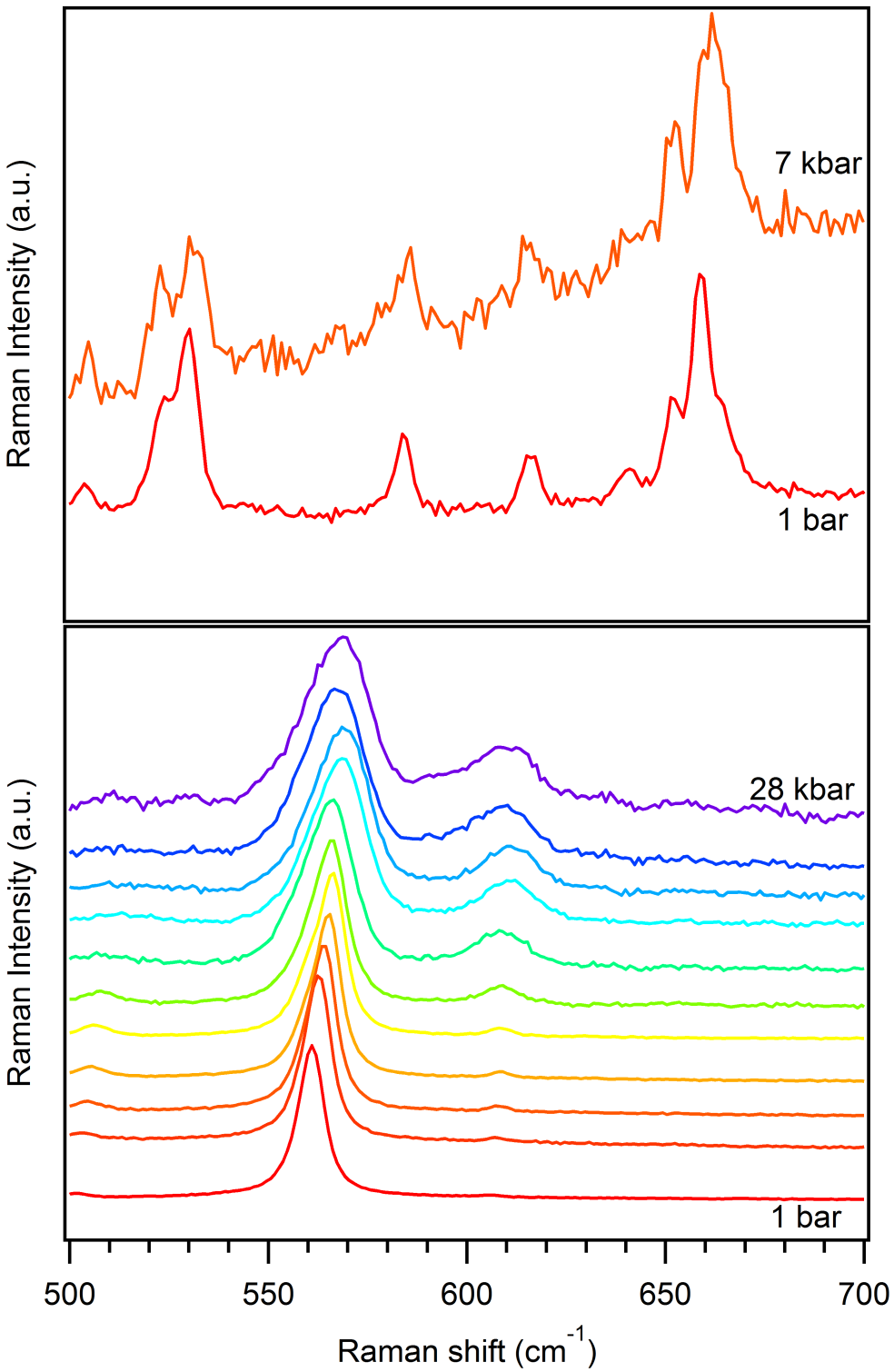

Figure S 11. Pressure-Dependent Raman spectra (λ_{exc} = 785 nm) of $[Au_2(dopdtc)_2]_n$ (Top panel) and of $[Au_2(edtc)_2]_n$ (Bottom panel)[4] for the 500 to 700 cm^{-1} region. Pressures for the bottom panel are (bottom to top): 1 bar, 4, 7, 9, 11, 13, 16, 19, 21, 24, 28 kbar. The bottom panel illustrates well the possible consequences of applying pressure on the linear polymeric chains of $[Au_2(edtc)_2]_n$ (broadening of the peaks as a result of structure degradation and appearance of a new peak at ca. 610 cm^{-1}).

Table S 3. Spectroscopic results (Diffuse reflectance and Luminescence) obtained for $[Au_2(dopdtc)_2]_n$ in contrast with compounds of the same type found in literature[4].

	$[Au_2(dopdtc)_2]_n$	**$[Au_2(edtc)_2]_n$**	**$[Au_2(edtc)_2]_n$ High pressure**	**$[Ag(edtc)]_6$**
E_{max} ambient conditions (cm^{-1})	14240	13750 18150	14000	12500
dE_{max}/dP (cm^{-1}/kbar)	-40	-120	-18	+17
FWHM ambient conditions (cm^{-1})	2718	1400	2750	≈3000
Reflectance (cm^{-1})	15322 16617 21290 (br)	17000 19500 >24 000		
E_{abs}-E_{lumi} (cm^{-1})	1082 2377 7050	3250 1350 --		

DFT Calculations: All the calculations were performed with the Gaussian 03 software (Gaussian Inc.)[12] on a tetrameric fragment, $[Au_2(dopdtc)_2]_2$ or $[Au_2(edtc)_2]_2$, of the corresponding polymeric gold (I) dithiocarbamate compound in the gas phase. First of all, a ground-state geometry optimization was performed on a tetrameric model of the polymer from the crystal structure geometric parameters (bond lengths, angles and dihedral angles, the crystal structure of $[Au_2(edtc)_2]_n$ was obtained from the literature[13]) with the Perdew-Burke-Ernzerhof exchange-correlation functional (PBEPBE)[14-16] and the relativistic basis set Lanl2dz with effective core potentials[17]. Then, from the optimized structure, molecular orbitals were calculated and excitation energies were evaluated by mean of the time-dependent density functional theory (TD-DFT) with the same functional and basis set. The molecular orbitals were visualized with the 5.08 release of the GaussView software (Gaussian Inc.)[12].

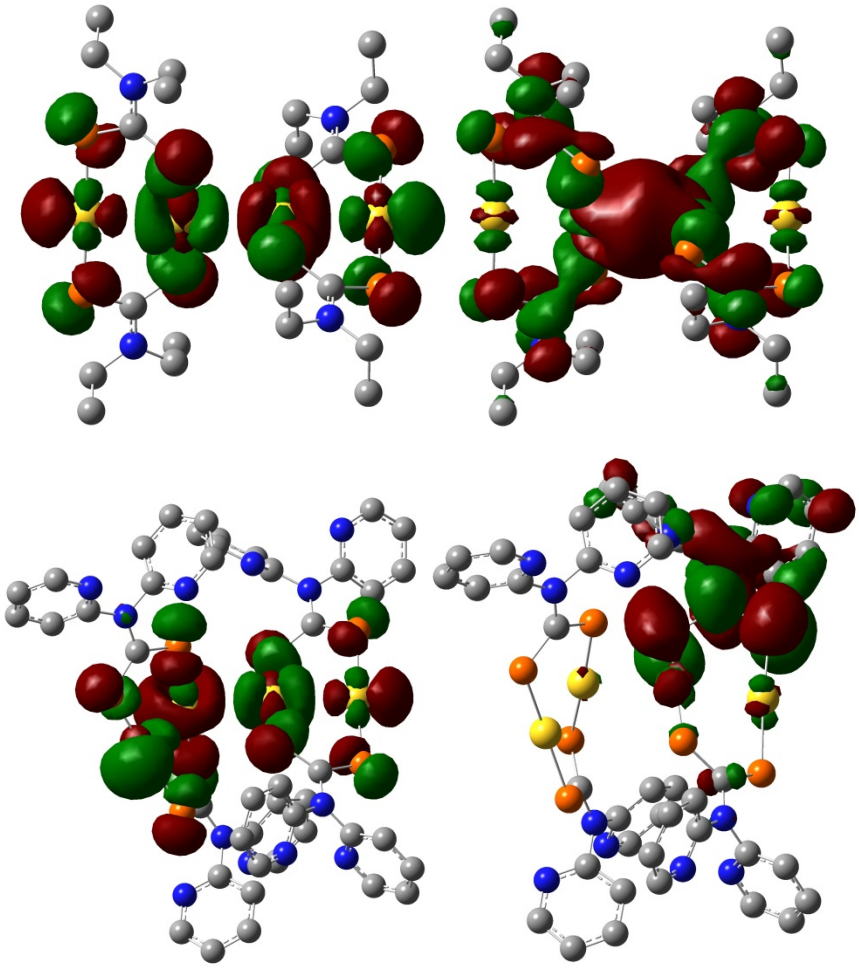

Figure S 12. Isodensity plots (0.02 atomic units) of HOMO (Left-hand side) and LUMO (Right-hand side) molecular orbitals for a linear gold (I) dithiocarbamate compound ($[Au_2(edtc)_2]_2$, upper panel) and for a "zig-zag" gold (I) dithiocarbamate compound ($[Au_2(dopdtc)_2]_2$, bottom panel). These were obtained from DFT calculations on a tetramer (PBEPBE[14-16]/Lanl2dz[17], Gaussian 03 (Gaussian Inc.)[12]) with the 5.08 release of the GaussView software (Gaussian Inc.)[12]. Hydrogens were omitted to clarify the picture. The color code used for the atoms is the following: Carbon: grey, Nitrogen: blue, Sulphur: orange and Gold: yellow.

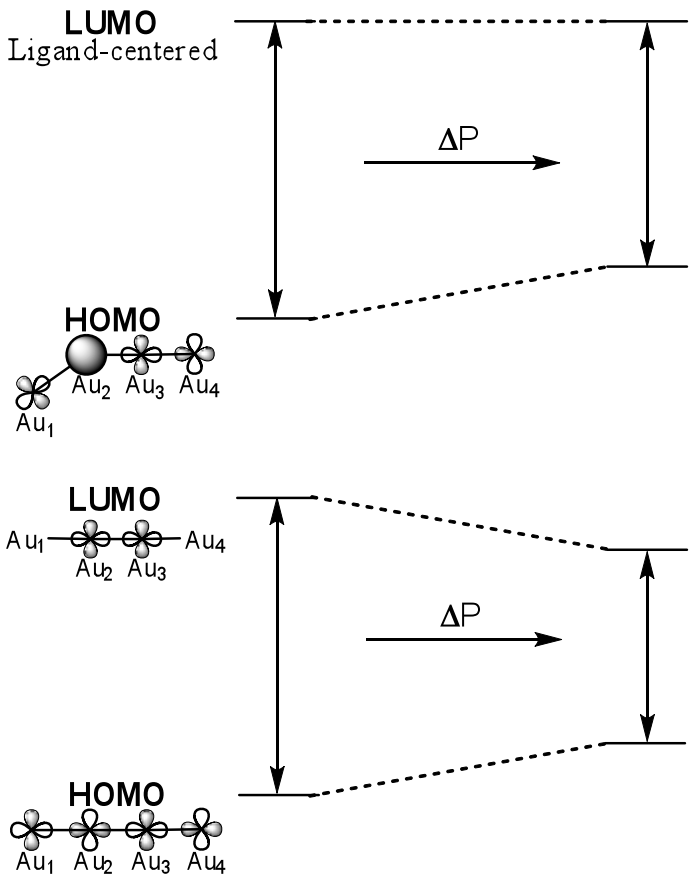

Figure S 13. Explanation of the observed Red-shift[4] with increasing pressure (Top: $[Au_2(dopdtc)_2]_2$ and Bottom: $[Au_2(edtc)_2]_2$). The following scheme highlights the fact that $[Au_2(dopdtc)_2]_2$ experiences a smaller red-shift with increasing pressure because of the nature of the LUMO orbital, which makes this orbital insensitive to a decrease of the interdimer Au-Au bond length.

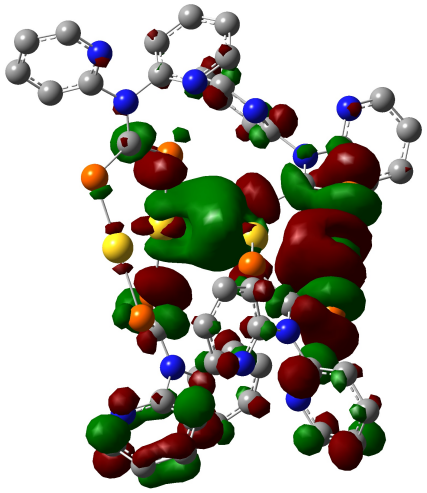

Figure S 14. Isodensity plots (0.02 atomic units) of the LUMO+16 molecular orbital of $[Au_2(dopdtc)_2]_2$ obtained from DFT calculations on a tetramer segment of the polymer(PBEPBE[14-16]/Lanl2dz[17], Gaussian 03 (Gaussian Inc.)[12]) with the 5.08 release of the GaussView software (Gaussian Inc.)[12]. Hydrogens were omitted to clarify the picture. The color code used for the atoms is the following: Carbon: grey, Nitrogen: blue, Sulphur: orange and Gold: yellow. This molecular orbital exhibits a Au-Au σ-bonding interaction between the dimers. The character of this interaction is really similar to what is found for the LUMO molecular orbital of another Gold(I) dithiocarbamate polymer[4], $[Au_2(edtc)_2]_2$.

Table S 4. First two theoretical excitation energies obtained from TD-DFT calculations (PBEPBE[14-16]/Lanl2dz[17], Gaussian 03 (Gaussian Inc.)[12]) made on the tetramer pre-optimized structure $[Au_2(dopdtc)_2]_2$.

	Transitions	Calculated ΔE (cm^{-1})	E_2-E_1 (cm^{-1})
$^1\Gamma$	HOMO to LUMO	13696	1292
	HOMO to LUMO+1	14989	
$^3\Gamma$	HOMO to LUMO	13354	1032
	HOMO to LUMO+1	14386	

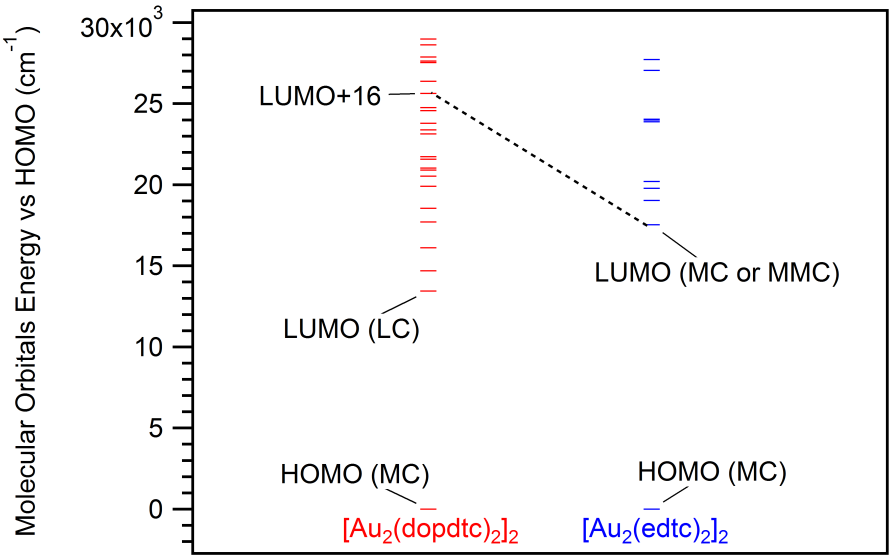

Figure S 15. Molecular Orbitals Energy diagram obtained from DFT calculations on tetramers of two Gold(I)dithiocarbamate polymer (PBEPBE[14-16]/Lanl2dz[17], Gaussian 03 (Gaussian Inc.)[12]). The dashed line illustrates the fact that the orbital with a similar character for the interaction between the dimers (σ-bonding) is higher in energy with respect to the HOMO for the studied system (red) than for a linear Gold(I)dithiocarbamate polymer (blue) found in literature[4].

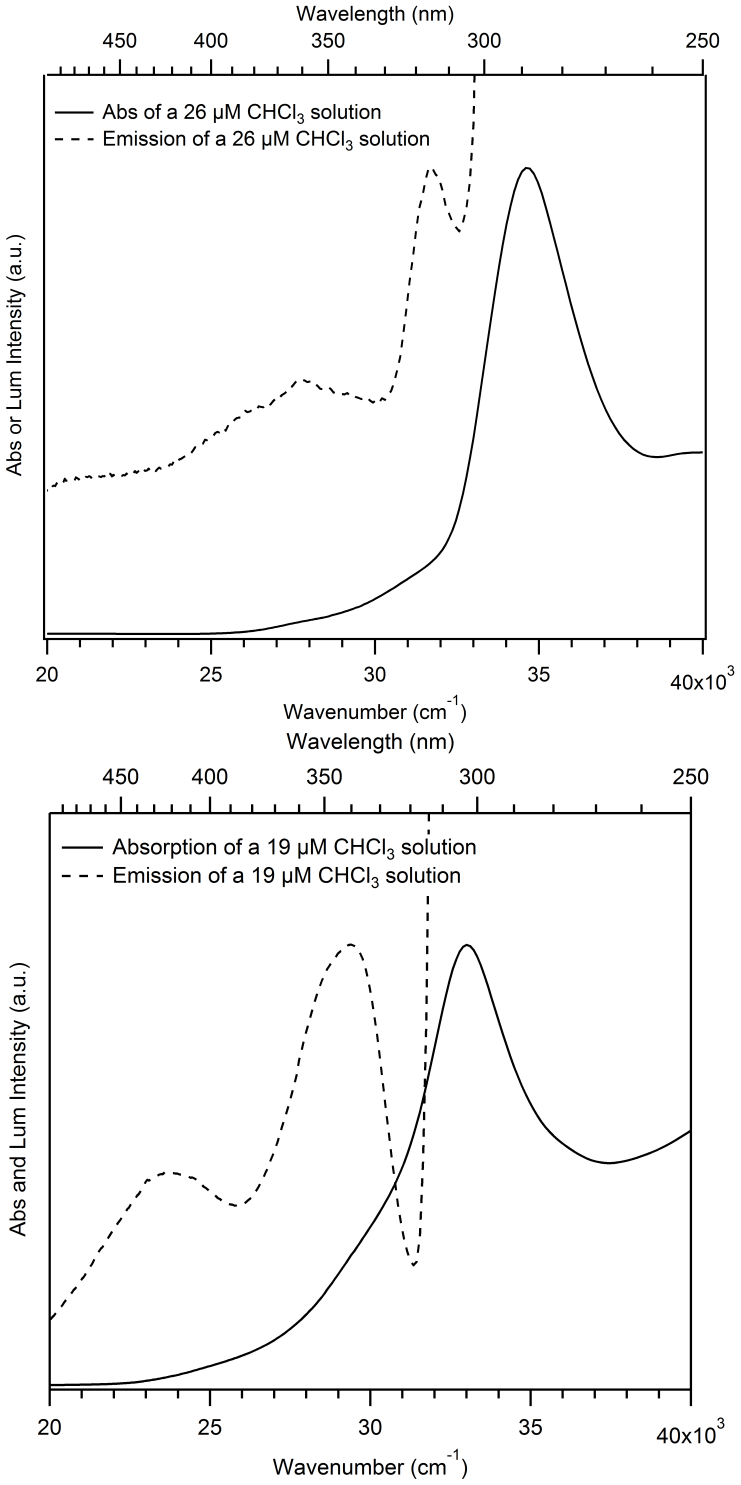

Figure S 16. Solution absorption and luminescence spectra of $[Au_2(edtc)_2]$ (top) and $[Au_2(dopdtc)_2]$ (bottom).

References

1. P. J. Bailey, R. A. Coxall, C. M. Dick, S. Fabre, L. C. Henderson, C. Herber, S. T. Liddle, D. Loroño-González, A. Parkin and S. Parsons, Chem. Eur. J. , 2003, 9, 4820.
2. R. Uson, A. Laguna, M. Laguna, D. A. Briggs, H. H. Murray and J. P. Fackler, *Inorg. Synth.*, John Wiley & Sons, Inc., 2007, pp. 85.
3. J. K. Grey and I. S. Butler, Coord. Chem. Rev., 2001, 219–221, 713.
4. F. Baril-Robert, M. A. Radtke and C. Reber, J. Phys. Chem. C, 2012, 116, 2192.
5. A. Altomare, G. Cascarano, C. Giacovazzo, A. Guagliardi, M. C. Burla, G. Polidori and M. Camalli, J. Appl. Crystallogr., 1994, 27, 435.
6. P. W. Betteridge, J. R. Carruthers, R. I. Cooper, K. Prout and D. J. Watkin, J. Appl. Crystallogr., 2003, 36, 1487.
7. L. Farrugia, J. Appl. Crystallogr., 1997, 30, 565.
8. T. D. Fenn, D. Ringe and G. A. Petsko, 2003, 36, 944.
9. F. Bonati and R. Ugo, J. Organomet. Chem., 1967, 10, 257.
10. D. C. Bradley and M. H. Gitlitz, J. Chem. Soc. A, 1969, 1152.
11. H. C. Brinkhoff and A. M. Grotens, Recl. Trav. Chim. Pays-Bas, 1971, 90, 252.
12. M. J. Frisch, G. W. Trucks, H. B. Schlegel, G. E. Scuseria, M. A. Robb, J. R. Cheeseman, J. J. A. Montgomery, T. Vreven, K. N. Kudin, J. C. Burant, J. M. Millam, S. S. Lyengar, J. Tomasi, V. Barone, B. Mennucci, M. Cossi, G. Scalmani, N. Rega, G. A. Petersson, H. Nakatsuji, M. Hada, M. Ehara, K. Toyota, R. Fukuda, J. Hasegawa, M. Ishida, T. Nakajima, Y. Honda, O. Kitao, H. Nakai, M. Klene, X. Li, J. E. Knox, H. P. Hratchian, J. B. Cross, V. Bakken, C. Adamo, J. Jaramillo, R. Gomperts, R. E. Stratmann, O. Yazyev, A. J. Austin, R. Cammi, C. Pomelli, J. W. Ochterski, P. Y. Ayala, K. Morokuma, G. A. Voth, P. Salvador, J. J. Dannenberg, V. G. Zakrzewski, S. Dapprich, A. D. Daniels, M. C. Strain, O. Farkas, D. K. Malick, A. D. Rabuck, K. Raghavachari, J. B. Foresman, J. V. Ortiz, Q. Cui, A. G. Baboul, S. Clifford, J. Cioslowski, B. B. Stefanov, G. Liu, A. Liashenko, P. Piskorz, I. Komaromi, R. L. Martin, D. J. Fox, T. Keith, M. A. Al-Laham, C. Y. Peng, A. Nanayakkara, M. Challacombe, P. M. W. Gill, B. Johnson, W. Chen, M. W. Wong, C. Gonzalez and J. A. Pople, *Gaussian 03*, (2004) Gaussian, Inc., Wallingford, CT.
13. D. D. Heinrich, J.-C. Wang and J. P. Fackler, Jnr, Acta Crystallogr., Sect. C: Cryst. Struct. Commun., 1990, 46, 1444.
14. M. Ernzerhof and G. E. Scuseria, J. Chem. Phys., 1999, 110, 5029.
15. J. P. Perdew, K. Burke and M. Ernzerhof, Phys. Rev. Lett., 1996, 77, 3865.
16. J. P. Perdew, M. Ernzerhof and K. Burke, J. Chem. Phys., 1996, 105, 9982.
17. P. J. Hay and W. R. Wadt, J. Chem. Phys., 1985, 82, 270.